

Improved operating space of the ICRF system in ASDEX Upgrade

V. Bobkov^{1,a)}, R. Bilato¹, H. Faugel¹, H. Fünfgelder¹, Ye. O. Kazakov²,
M. Mantsinen^{3,4}, J.-M. Noterdaeme^{1,5}, R. Ochoukov¹, Th. Pütterich¹,
G. Suárez López¹, W. Tierens¹, W. Zhang¹, the ASDEX Upgrade Team
and the EUROfusion MST1 Team^{b)}

¹Max-Planck-Institut für Plasmaphysik, Boltzmannstr. 2, 85748 Garching, Germany

²LPP-ERM/KMS, Royal Military Academy, 30 Avenue de la Renaissance B-1000, Brussels, Belgium

³Barcelona Supercomputing Center, Barcelona, Spain

⁴ICREA, Barcelona, Spain

⁵Applied Physics Department, University of Ghent, Ghent, Belgium

^{a)}Corresponding author: bobkov@ipp.mpg.de

^{b)}See the author list of H. Meyer et al. 2017 Nuclear Fusion 57,102014

Abstract. Following the improvements of compatibility of ICRF system with the tungsten (W) wall in ASDEX Upgrade (AUG) by using the boron-coated limiters on the 2-strap ICRF antennas and the 3-strap antennas with the W-limiters, the ICRF operating space was further extended in 3 areas: power, phase control between the antennas and frequency range. The available ICRF power in AUG was increased by using an additional RF generator to feed the central straps of the 3-strap antennas which require a 1.5:1 or 2:1 power ratio between the central strap and the two outer straps (combined) to minimize the ICRF-specific W sources. This increases the total experimentally achievable launched ICRF power in the optimized configuration to ~ 5.7 MW. A new phase control system enabled phase-locked operation of all 4 AUG ICRF antennas. This allows a better control of the launched k_{\parallel} spectrum which on its turn is modified when both neighboring antennas are active, as well as of the structure of the global RF field distribution within the AUG vessel. Measurements by the RF magnetic field (B-dot) probes show that the RF field distribution can indeed be significantly affected by the variation of the phasing between the ICRF antenna pairs. However its effect on the core plasma and on the residual ICRF specific plasma-wall interactions is small, for the cases so far limited to the H-modes at medium plasma densities. The available frequency range was extended and now covers four discrete frequencies (f): 30.0, 36.5, 41.8 and 55.1 MHz. In addition to the standard hydrogen (H) minority in deuterium (D) on-axis heating scheme at the magnetic field (B_t) of 2.0, 2.5, 2.8 and 3.1 T, the RF frequency range allows the use of the 3-ion D-(³He)-H and ⁴He-(³He)-H heating schemes at $B_t=2.5-3.1$ T ($f=30$ MHz – off-axis and on-axis), on-axis $3\omega_c$ D heating at $B_t=1.9$ T ($f=41.8$ MHz) and at $B_t=2.5$ T ($f=55.1$ MHz) and $2\omega_c$ H heating at $B_t=1.9$ T ($f=55.1$ MHz).

EXTENTIONS OF ICRF SYSTEM IN ASDEX UPGRADE

After the compatibility of the ICRF heating with the tungsten (W) wall of ASDEX Upgrade (AUG) has been improved by using the boron-coated limiters on the 2-strap ICRF antennas and the 3-strap antennas with the W-limiters [1], the ICRF operating space could be further extended by: a) increasing the available generator power; b) improving the phasing control; and c) extending the frequency range.

The AUG ICRF system consists currently of 4 antennas (named $a1\dots a4$), powered by 5 generators (named $g1\dots g5$). Starting from the beginning of 2019, generator $g5$ - the old ASDEX/W7-AS ICRF generator converted to the final stage tetrode EIMAC 4CM2500KG [2], was integrated into the AUG operation for frequencies $f > 33$ MHz. This increased the power from the 3-strap antennas ($a2$ and $a4$) in the optimized configuration [1] with the power ratio between the central and the outer straps 1.5:1 or 2:1 to minimize the ICRF-specific W sources. Figure 1 shows the scheme of $g5$ connections. The realistically available total ICRF power for $f = 36.5$ MHz was thus increased

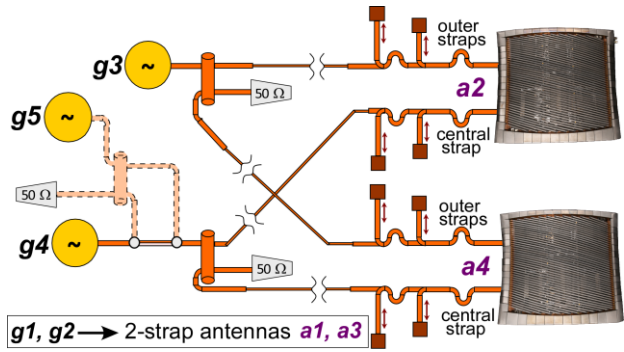


FIGURE 1. The AUG 3-strap antenna circuit layout.

strap and the inter-antenna phasing control are prioritized to decrease the system reaction time down to $\sim 150 \mu\text{s}$ for a 180° span and allow better phasing control during plasma transients. Arbitrary waveforms of the strap phasing and the inter-antenna phasing can be programmed. The antennas are equipped with a number of diagnostics to characterize antenna-plasma interactions and wave propagation [6].

The ICRF frequency range was extended to cover 55.1 MHz in addition to the previously used 30 MHz, 36.5 MHz and 41.8 MHz, enabling the formerly inaccessible central 3rd harmonic deuterium (D) acceleration at $B_t = 2.5 \text{ T}$. At the same time, the core 2nd harmonic H heating was made possible at $B_t = 1.8 \text{ T}$ and $f = 55.1 \text{ MHz}$.

RESULTS

Experimental validation of the phase-locked control scheme with 5 generators at high ICRF power (P_{ICRF}) from all antennas is presented in Fig. 2 for the H-minority heated AUG discharge #36022 with $I_p = 0.8 \text{ MA}$ and $B_t = 2.5 \text{ T}$. Three steps of P_{ICRF} with the maximum above 5 MW including contributions from g_3 , g_4 and g_5 (see time traces in Fig. 2), are applied in addition to 2.5 MW NBI (switched on at 0.9 s) and approximately 2 MW ECRH power (ramped up from 0.45 s). The plasma stored energy W_{MHD} and neutron rate increase in accordance with the ICRF power. In this discharge with moderate gas puff and plasma density, the main chamber radiated power P_{rad} increases only slightly when P_{ICRF} is increased, although the wall conditions can be considered as unboronized (about 100 discharges after boronization). During the short ramp-ups of P_{ICRF} , the inter-antenna phasing is kept constant. During each of the P_{ICRF} plateaus, the inter-antenna phasing is scanned by 360° , whereas the strap phasing of the 3-strap antenna a_4 (and that of a_2 by equivalent transmission line lengths and RF matching) is maintained constant in dipole phasing (measured 0°).

In the lower graph of Fig. 2, the W influx measured at the a_4

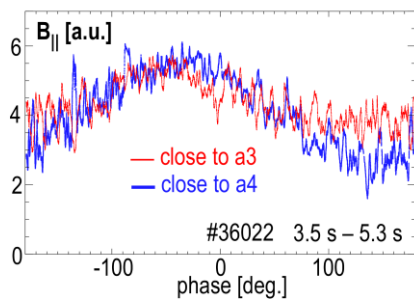


FIGURE 3. B-dot probe measurements from two locations between a_3 and a_4 as a function of inter-antenna phase.

from $\sim 4.5 \text{ MW}$ to $\sim 5.7 \text{ MW}$. The available power is also affected by aging g_1 - g_4 [4], in particular the final stage BBC CQK650-2 tetrodes. A newly built phase control system allows phase-locked operation of all antennas, with simultaneous control of 4 phase values: phase between RF voltages at the 3dB g_1/g_2 and g_4/g_5 combiners, phase between RF currents of the a_4 straps and the inter-antenna phase [5] between the forward power measured at neighboring antennas a_3 and a_4 . The phase control uses the low-latency parallel X MOS XS1 controller architecture [3] linked to the Direct Digital Synthesizers (DDS) based on an AD9959 reference board. The antenna

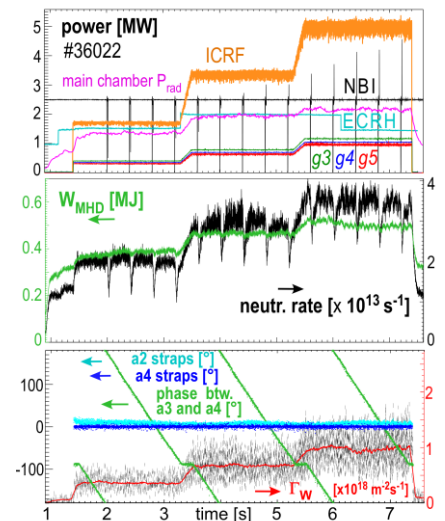


FIGURE 2. Time traces of #36022 with high ICRF power and inter-antenna phase scans.

limiter closest to a_3 is shown (black) together with its time-averaged behavior (red curve). In contrast to the measurements in similar discharges in the past when all antennas were 2-strap antennas [5], no noticeable effect of the inter-antenna phase on the W source is measured in otherwise constant phases of the discharge. The same applies to all the antenna W source measurements, to the core W content (not shown), and to the core plasma parameters. The likely contributing factor to this is that the W source were significantly reduced and the superposition of the RF and the DC effects in the scrape-off-layer [7] imposed by two neighboring antennas were changed after the installation of the 3-strap antennas, since the 20%-30% variation of the W source and the W content have been conducted in [5]. On the other hand, the phase variation was not studied in low gas / low density scenarios so far where the effect could be stronger.

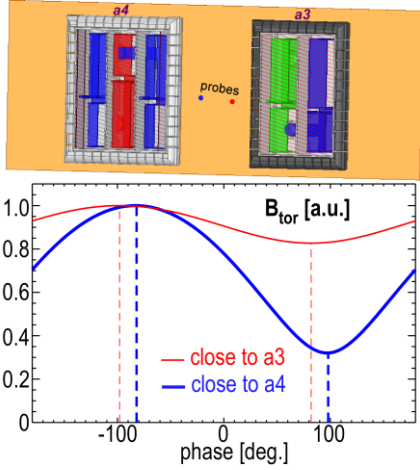


FIGURE 4. HFSS calculations corresponding to the measurements in Fig. 3.

can experience significant changes when both neighboring antennas are powered. Generally speaking, the launched spectrum does not necessarily consist of independent contributions of the 3-strap and of the 2-strap antennas, but rather of a 5-strap array with a variety of the strap distances. Figure 5 presents the calculations of the k_{\parallel} spectrum using the model presented in Fig. 4, for several cases with the dipole internal strap phasing: for a 2-strap antenna operating alone (averaged $k_{\parallel} \approx 7.5 \text{ m}^{-1}$), for a 3-strap antenna alone with the standard 2:1 strap power ratio (averaged $k_{\parallel} \approx 11 \text{ m}^{-1}$), as well as for the cases when two antennas operate simultaneously. For the latter, the spectrum depends on the inter-antenna phase and manifests itself in 4 or 5 peaks around the average $k_{\parallel} \approx 9.5 \text{ m}^{-1}$ between the two antennas. These peaks can in principle be understood as beatwaves in real space between the k_{\parallel} modes

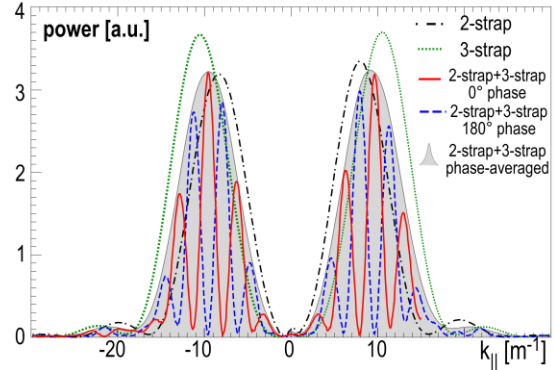


FIGURE 5. k_{\parallel} spectrum of 2-strap, 3-strap and synchronous antenna operation.

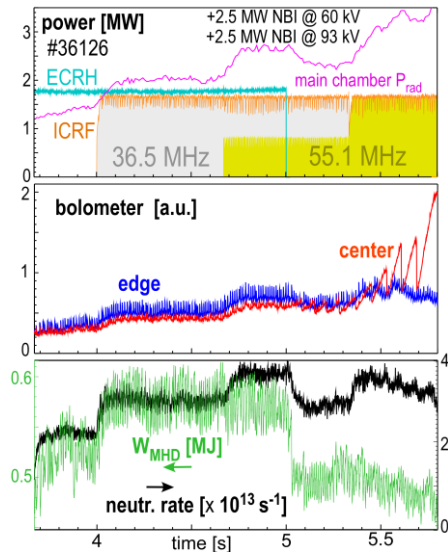


FIGURE 6. Combined H-minority/2nd harmonic D heating at 36.5 MHz and 3rd harmonic D at 55.1 MHz.

Nevertheless the inter-antenna phase affects significantly the RF field distribution close to and between the antennas. Figure 3 shows the fast wave amplitude of the magnetic field measured by two of the B-dot probes in the locations of the two ends of the probe array [8] between $a3$ and $a4$. The measured parallel RF magnetic field experiences a period of amplitude modulation during the phase scan. This period is qualitatively reproduced in electromagnetic calculations by the HFSS code using a two-antenna model with a lossy dielectric as antenna loading (see upper side of Fig. 4 and more details of the load setup in [5]). The toroidal component of magnetic field calculated in the locations of the probes corresponding to the experiment is presented in Fig. 4 as a function of the inter-antenna phase. The minima and the maxima of the magnetic field are shifted when comparing one location with the other, similarly as in the experiment (Fig. 3). The shape of the phase dependency is not sinusoidal, likely due to the fact that several spatial modes influence the local field. This picture is consistent with the fact that k_{\parallel} spectrum

produced by the two antennas. The counter-intuitive irregular structure of the k_{\parallel} spectrum can be of importance when considering wave propagation and absorption. However, as is mentioned above, no clear effect of the inter-antenna phase (and spectrum) variation has been observed so far in the core of the H-minority heated discharges. In the default ICRF configuration, the two antennas are operated at a frequency difference of 1 kHz, chosen in the past to avoid uncertainties of the inter-antenna phasing. This effectively makes multiple fast sweeps of the inter-antenna phase during every ICRF pulse. The phase-averaged k_{\parallel} spectrum representative for this case is shown in Fig. 5 (grey color) with a single broad peak and averaged $k_{\parallel} \approx 9.5 \text{ m}^{-1}$.

In addition to the 41.8 MHz option for the 3rd harmonic D acceleration [9], the extension of the frequency range to cover 55.1 MHz allowed this scenario to perform at $B_t = 2.5 \text{ T}$, compatible with the central ECRH and the standard H minority/2nd harmonic D ICRF heating scheme at 36.5 MHz. Figure 6 shows an example of such combination for $I_p = 1 \text{ MA}$ so-called “standard H-Mode” AUG discharge #36126, on top of 5 MW NBI power injected by one 60 kV and one 93 kV beam. The ICRF power is kept constant around 1.6 MW and starts with the single frequency of 36.5 MHz at $t = 4.0 \text{ s}$. It transits to the double 36.5 MHz / 55.1 MHz frequency heating at $t = 4.67 \text{ s}$, increasing the neutron rate and keeping the stored plasma energy. When ECRH is

switched off, the neutron rate and the stored energy decreases, but the discharge is still stable radiatively as indicated by the signals of the central and the edge bolometer lines of sight, whereas the sawteeth become pronounced. When at $t = 5.33$ s the pure 55.1 MHz power takes over, the sawteeth period increases from 70 ms to above 100 ms which is remarkable for this high density scenario. The neutron rate increases too, but the stored energy (as likely the heating efficacy) degrades and the discharge experiences radiation instability. To summarize, the mixture of the 2nd and 3rd harmonic of D in combination with ECRH provides a powerful tool for tailoring the fast D population and

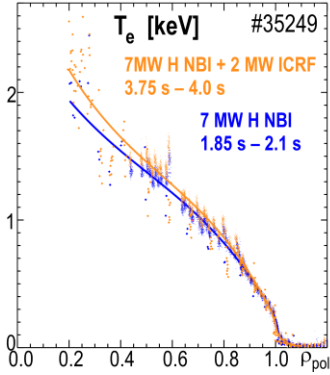


FIGURE 7. Change of T_e during ICRF using 3-ion scheme in ${}^4\text{He}$ - ${}^3\text{He}$ -H mixture.

sawteeth properties. However further studies including the theoretical description of the double frequency heating are required.

The first attempts to study the ITER-relevant 3-ion ${}^4\text{He}$ - ${}^3\text{He}$ -H heating scenario were made recently. The ${}^3\text{He}$ fueling recipe was taken from the successful preceding 3-ion ICRF experiments in AUG H-D plasmas [10], with magnetic field between $B_t=2.5$ T and $B_t=3.1$ T (shifting the ${}^3\text{He}$ resonance position from HFS off-axis towards mostly on-axis) and ${}^3\text{He}$ concentration $0.5\% < c_{3\text{He}} < 2\%$. In discharge #35249 ($B_t = 2.9$ T), ${}^4\text{He}$ concentration was scanned between 8% and 17%, and a maximum in stored energy and an increase in electron temperature T_e (not measured for $\rho_{\text{pol}} < 0.2$) were observed when compared to the phases with hydrogen NBI only. The increase of T_e is shown in Fig. 7 with raw data and fits made using the same boundary conditions. Further development of this scenario is planned in the future.

SUMMARY

Flexibility of the AUG ICRF system was improved by increasing the power which can be launched by the 3-strap antennas by using an additional RF generator which feeds the central straps, providing the possibility for a phase-locked operation of all antennas and introducing 55.1 MHz in the operational frequency range. The synchronous antenna operation allows a more precise control of the two-antenna spectrum which generally constitutes several peaks around the averaged value of k_{\parallel} between the two antennas. In addition, control of the local RF fields in the torus vessel is possible which in many cases can qualitatively be described by EM calculations with a simplified geometry and antenna loading. A large variety of heating scenarios can be covered by the AUG ICRF system: standard hydrogen (H) in deuterium (D) minority on-axis heating scheme at B_t of 2.0, 2.5, 2.8 and 3.1 T, D- ${}^3\text{He}$ -H and ${}^4\text{He}$ - ${}^3\text{He}$ -H 3-ion schemes at $B_t = 2.5$ -3.1 T ($f=30$ MHz – off-axis and on-axis), on-axis $3\omega_c$ D heating at $B_t=1.8$ T ($f=41.8$ MHz) and at $B_t=2.5$ T ($f=55.1$ MHz) and $2\omega_c$ H heating at $B_t=1.8$ T ($f=55.1$ MHz). Recently, the 3rd harmonic D scenario at $B_t=2.5$ T was successfully tested which can be used in combination with the standard H minority / 2nd harmonic D heating to have more control of the D fast ion population. Progress in assessing the ${}^4\text{He}$ - ${}^3\text{He}$ -H heating scheme was made after the D- ${}^3\text{He}$ -H scheme has been tested in a broad range of conditions.

ACKNOWLEDGMENTS

This work has been carried out within the framework of the EUROfusion Consortium and has received funding from the Euratom research and training programme 2014-2018 and 2019-2020 under grant agreement No 633053. The views and opinions expressed herein do not necessarily reflect those of the European Commission.

REFERENCES

1. V. Bobkov et al., *Plasma Phys. Control. Fusion* **59** (2017) 014022.
2. H. Fuenfgelder et al., *AIP Conference Proceedings* **1406** (2011) 121.
3. D. May, *IEEE Micro* **32** (2012) 6, pp. 28-37.
4. H. Faugel et al., “The prospects of ICRF generators”, P2.17, *this conference*.
5. V. Bobkov et al., *Nucl. Fusion* **53** (2013) 093018.
6. H. Faugel et al., *Fus. Eng. Des.* (2019), in press, <https://doi.org/10.1016/j.fusengdes.2019.04.040>
7. V. Bobkov et al., *Nucl. Mat. Ener.* **18** (2019) 131–140.
8. R. Ochoukov et al., *Rev. Sci. Inst.* **86** (2015) 115112.
9. M. Mantsinen et al., *Proceedings of 43rd EPS Conference on Plasma Physics*, P1.035.
10. Ye. Kazakov et al., *Proc. 27th Int. Conf. on Fusion Energy* (2018), Ahmedabad, India, EX/8-1.